Proceedings of the 4th International Conference on Machine Learning and Automation
DOI: 10.54254/2755-2721/2026.38120

Mechanical Structure Design and Simulation Analysis of a Dual-Axis Solar Tracking System

Chenyang Ran

School of Mechanical and manufacturing Engineering, UNSW Sydney, Sydney, Australia
z5664398@ad.unsw.edu.au

Abstract. This paper presents the mechanical design and static structural assessment of a gear driven dual axis solar tracking system. Independent azimuth and elevation mechanisms are used to orient the photovoltaic module, while a compact gear train transfers motor torque through the support structure to the base. A three dimensional model is developed in SolidWorks, and the upper support is evaluated with a finite element model whose material properties, restraints and loads follow the actual mounting arrangement. Panel self weight is examined as a baseline condition, and a second case introduces natural wind loading. Von Mises stress, total deformation and factor of safety are used to evaluate structural performance. The baseline solution shows small stress and displacement, and the combined case is defined as the main condition for final strength verification and design refinement.

Keywords: dual axis solar tracking, mechanical design, finite element analysis, static structural analysis, wind loading

1. Introduction

Solar photovoltaic output is sensitive to the angle of incoming sunlight. Because the sun moves continuously across the sky, a fixed panel is close to its preferred orientation only for part of the day. A dual-axis tracker corrects this mismatch through independent azimuth and elevation motions. Tracking accuracy is important, but reliable long-term operation also depends on the mechanical structure. The support frame carries panel weight and wind load, the shafts and gears transfer motion, and the base must resist both vertical force and overturning moment. For this reason, the tracker is treated here as a combined structural and transmission design problem rather than only a control problem.

Chinese studies have explored several practical routes for dual-axis tracking. Liu et al. [1] developed a two-axis sun-tracking PV system based on coordinated azimuth and elevation control. Ren [2] introduced IoT functions into a coupled tracking system, extending the design beyond motion control to data exchange and operation management. Fang et al. [3] used an STM32 controller, a common choice for compact tracking devices, while Liu et al. [4] applied Fourier fitting to reduce the burden of real-time angle calculation. Li and Li [5] combined control with a physical dual-axis tracking device. Taken together, these studies cover controller selection, angle calculation, networking and system implementation. Mechanical load paths and long-term structural response, however, receive less attention, which motivates the structural emphasis of this study.

© 2026 The Authors. This is an open access article distributed under the terms of the Creative Commons Attribution License 4.0 (https://creativecommons.org/licenses/by/4.0/).

DOI: 10.54254/2755-2721/2026.38120

International research has broadened the topic to positioning, control comparison, condition monitoring and system integration. Wu et al. [6] used a satellite compass and inclinometer for automatic orientation. Mamodiya and Tiwari [7] compared several control strategies, shifting the discussion from a single controller to relative performance. Pirayawaraporn et al. [8] investigated sensorless tracking, showing the interest in reducing hardware dependence. Flores-Hernández et al. [9] linked real-time monitoring with service life, while Paliyal et al. [10] reviewed the wider development and remaining challenges of automatic solar trackers. Acosta-Banda et al. [11] combined embedded control with machine vision. These studies show a clear move from isolated tracking functions toward integrated control, monitoring and mechanical validation.

Mechanical design and simulation are more directly relevant to the present work. Shang and Shen [12] demonstrated a complete dual-axis tracking structure and system, confirming that a clear mechanical layout is essential for two-degree-of-freedom motion. Alexandru [13] optimized the mechanism from the viewpoint of kinematics and actuator placement, showing that actuator position, transmission path and geometry affect tracker performance. Chen et al. [14] incorporated CAD modelling and structural verification into the development of a manufacturable tracker. Saber et al. [15] combined mechanism design, dynamic simulation and prototype testing. These studies make it clear that the mechanical structure is not merely a carrier for the control system; it directly influences motion accuracy, actuator load and service reliability.

Dual-axis trackers vary widely in support layout, transmission method, dimensions and installation conditions, so structural results from one design cannot simply be transferred to another. This work therefore develops a gear-driven mechanism and builds the azimuth stage, elevation stage, panel support, shafts and base as one consistent 3D design. A static finite-element model is then created from the actual mounting arrangement. The first load case includes structural and panel self-weight, followed by a combined case with natural wind. Structural performance is evaluated using von Mises stress, total deformation and factor of safety. The aim is to connect mechanical design, load transfer and finite-element verification in a form that can guide later prototype manufacture and refinement.

2. Mechanical structure design of the dual-axis solar tracking system

2.1. Overall structure and working principle

The tracker consists of a PV module, panel support, left and right brackets, an azimuth rotation stage, an elevation shaft, geared motors, a gear transmission and a base. The panel is fixed to the upper support, which is connected to the side brackets through a horizontal shaft so that the panel can change its tilt angle. The side brackets are mounted on the lower azimuth stage, which is supported by the base and rotates the complete upper assembly about a vertical axis. This layered arrangement separates the two rotational degrees of freedom and simplifies assembly, maintenance and later static modelling [12, 14]. The upper structure must hold the panel while leaving room for the elevation shaft, bearings and drive connection. The lower stage carries most of the upper mass and transfers it to the base, so both levels must combine rotational freedom with adequate stiffness.

Figure 1 shows the overall 3D model of the dual-axis solar tracking system.

DOI: 10.54254/2755-2721/2026.38120



Figure 1. Overall 3D model of the dual-axis solar tracking system

During azimuth adjustment, a geared motor drives the lower rotating stage through the gear pair, causing the upper frame and panel to turn about the vertical axis. Elevation is controlled by a separate drive acting on the horizontal shaft, which tilts the panel upward or downward. The two motions may be commanded independently or coordinated according to solar position. Because solar tracking is slow and intermittent, a geared motor and gear train provide the required low output speed and higher torque without a complex transmission. The fixed gear geometry also helps maintain alignment and makes interference checks straightforward in the 3D assembly. In operation, the azimuth stage sets the general horizontal orientation and the elevation stage then corrects panel tilt.

Bearings at both ends of the elevation shaft reduce rotational resistance and constrain the shaft position. The side brackets provide the bearing seats and carry the panel and upper frame, so their height, thickness and connection geometry must balance strength with assembly clearance. The lower azimuth stage carries the PV module, upper frame, elevation shaft and part of the transmission. Motors and gears are therefore placed close to their respective axes to limit additional bending caused by drive-component weight, while sufficient clearance is retained for bearings, fasteners and the gear set. A relatively broad base connects the rotating structure to the foundation and provides a stable path for the upper loads.

Panel weight and wind load act first on the upper panel support, then pass through the elevation shaft into the side brackets. From there, the load is transferred to the azimuth stage and finally into the base and foundation. Gear meshing introduces additional forces at the shafts and support locations, making the shaft holes, bearing seats, bracket roots and base mounting region important inspection points. This direct load path makes it easier to define realistic loads and constraints in the finite-element model. Excessive local compliance could also disturb shaft alignment or gear meshing, so both strength and deformation must be considered.

2.2. Key components and structural design

Once the motion concept was fixed, the detailed design focused on support, transmission and installation. The upper frame holds the panel and provides the basis for elevation motion. Shafts and gears transmit motor torque, the side brackets locate the bearings and carry the upper load, and the

DOI: 10.54254/2755-2721/2026.38120

base connects the azimuth stage to the foundation. Interference must be avoided throughout the motion range, while the gear pair, shafts and bearings must retain a sensible geometric relationship. Keeping the drive close to the rotational axes shortens the transmission path and reduces parasitic bending. Similar layout considerations are reported in other dual-axis tracker studies [13, 15]. Figure 2 separates the assembly into the upper support/elevation section and the lower drive/azimuth section and labels the main parts for reference.

In Figure 2, item 1 is the PV module, which receives solar radiation and is also the main external load on the upper structure. Item 2 is the elevation shaft; together with the two bearings, it allows the panel and its connecting frame to rotate about a horizontal axis. Item 3 is the pair of support brackets. These brackets house the bearings, support the elevation shaft and transfer the upper loads to the lower stage. During elevation motion, the panel and upper frame rotate as one assembly while the side brackets remain fixed, so the brackets carry vertical load, wind-induced lateral load and local reactions from the shaft. Item 4 is the azimuth rotation mechanism between the upper and lower sections. Its vertical-axis rotation changes the horizontal direction of the entire upper assembly. Item 5 is the drive motor, which delivers low-speed torque through the reduction and gear stages. Item 6 is the base, which anchors the mechanism and resists vertical load and overturning tendency. The overall motion is the superposition of two independent rotations: azimuth sets the horizontal direction and elevation sets the panel tilt.

The design uses a 2000 mm × 1000 mm PV module with a mass of 30 kg, giving a panel area of 2 m². The output shaft carries gear torque and support reactions and is specified as 45 steel. The gears use 40Cr to provide adequate strength and wear resistance. Q235 structural steel is used for the side brackets, which are the main focus of the later static analysis, while the base is HT200 cast iron. A 3:1 gear ratio provides an additional speed reduction and torque increase after the motor gearbox. These materials and transmission choices are conventional and readily compatible with common manufacturing and assembly methods.

The main panel-connection bracket is approximately 222 mm × 80 mm × 8 mm, which provides the required interface with the upper shaft and connecting parts. The output shaft is about 78 mm long, leaving sufficient axial space for the gear, bearings and adjacent components. A gear centre distance of roughly 70 mm defines the relative position of the driving and driven gears. The base has a main diameter of about 160 mm, providing a useful mounting footprint without making the lower assembly unnecessarily large. Table I summarises these dimensions and materials; it is intended only as a quick reference and does not introduce additional design values.

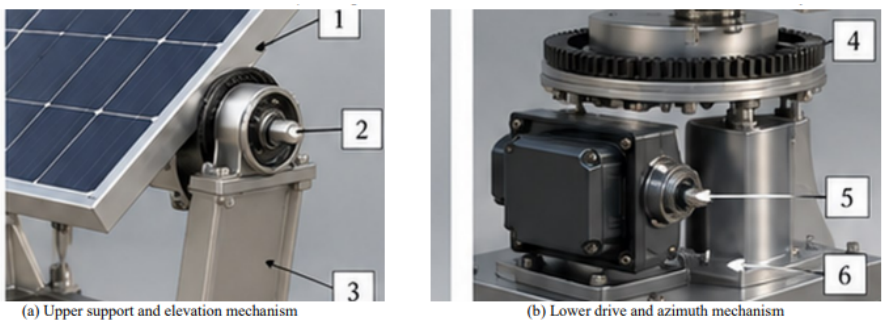


Figure 2. Main mechanical structure of the dual-axis tracker: (a) upper support and elevation mechanism; (b) lower drive and azimuth mechanism

Labels: 1 - PV module; 2 - elevation shaft; 3 - left/right support brackets; 4 - azimuth rotation mechanism; 5 - drive motor; 6 - base.

DOI: 10.54254/2755-2721/2026.38120

Placing the drive close to the rotation axis shortens the torque path and reduces extra bending from motor and gear weight. The bearing seats and shaft holes should remain well aligned; otherwise, assembly errors can introduce shaft bending, higher friction and local stress. The bracket-to-lower-stage interface also needs sufficient contact area so that load is not concentrated over a narrow region. Base mounting holes both fix the structure and transfer load into the foundation, making the hole surroundings and the support-column root important inspection areas. If the static analysis later identifies excessive stress in these locations, larger fillets, local thickening or reinforcing ribs can be introduced.

The tracker is composed mainly of plates, brackets, shafts, gears, bearings and standard fasteners, with no unnecessary complex surfaces or special joints. Bracket components can be produced by conventional cutting, machining and welding, while the shafts and gears use standard machining processes. Off-the-shelf bearings and bolts also simplify later replacement. Assembly begins from the base, followed by the azimuth stage and drive, then the side brackets, elevation shaft and upper panel support. This sequence makes it easier to check shaft alignment and gear meshing step by step. At this stage, the motion relationships, key dimensions and load path are sufficiently defined to support the finite-element boundary conditions used in the next section.

After assembly, interference between the two rotational degrees of freedom must also be checked. During elevation motion, adequate clearance is required between the panel frame and the side brackets, particularly at larger tilt angles. During azimuth rotation, the upper support, motor housing and gear set must have enough free space so that cables, fasteners and bracket edges do not restrict movement. The two bearing holes should share the same axis, and the gear centre distance should remain close to its design value to maintain proper tooth engagement. These checks can be completed in the 3D assembly before manufacture, reducing the need for repeated physical modification. They are also closely related to structural analysis, because realistic load transfer depends on correct alignment, clearance and connection geometry.

Table 1. Main structural parameters of the dual-axis tracking system

Item	Main parameter
PV module	2000 mm × 1000 mm, 30 kg
Panel support	Approx. 222 mm × 80 mm × 8 mm
Output shaft	Approx. 78 mm, 45 steel
Gear transmission	Ratio 3:1, centre distance approx. 70 mm
Side brackets	Q235 structural steel
Base	HT200, main diameter approx. 160 mm

3. Static simulation and structural analysis

The upper panel-support structure is selected for static analysis because it carries the panel load and transfers it into the lower mechanism. The geometry is simplified from the SolidWorks model by retaining the support plates, uprights, shaft holes and major connection regions while removing small chamfers, decorative details and non-load-bearing features. This reduces the mesh size without changing the main load path and keeps the analysis focused on the shaft holes, connecting plates and lower mounting region. A baseline case first includes structural and panel self-weight. A second case retains the same constraints and adds natural wind. This approach follows the virtual-prototyping

DOI: 10.54254/2755-2721/2026.38120

and structural-verification methods commonly used for dual-axis trackers [13, 15]. The model assumes linear elasticity and small deformation and evaluates von Mises stress and total deformation; plasticity, fatigue and transient impact are outside the present scope.

3.1. Finite element model and simulation conditions

The analysed component is the upper panel support, modelled as Q235 structural steel with an elastic modulus of 2.06×10^{11} Pa, Poisson's ratio of 0.30, density of 7850 kg/m³ and yield strength of 235 MPa. The material is treated as isotropic and linearly elastic. The mounting surfaces at the lower end of the support are fixed to approximate the restraint provided by the bolted connection and lower structure in the real assembly. Only the actual mounting regions are constrained, avoiding an unrealistically stiff model. Combining mechanical modelling with structural verification in this way is also consistent with recent dual-axis tracker studies [14, 15].

The PV module is 2000 mm × 1000 mm with a mass of 30 kg and an area of 2 m². Using g = 9.81 m/s², its weight is approximately 294 N. Because the full panel is not included in the finite-element model, this weight is transferred as an equivalent load through the upper support and shaft locations, while the support structure itself is subjected to gravity. A 30° panel angle is selected as a representative operating condition. It is used only as a repeatable static case and does not represent the mechanical travel limit. At this inclination, the panel weight produces different load components and a moment around the elevation shaft, making the condition more useful than a fully horizontal position for examining the support connections.

The combined case adds a natural wind load to self-weight. A wind speed of 15 m/s is used with an air density of 1.225 kg/m³, a drag coefficient of 1.2 and a 2 m² projected panel area. With the simplified equivalent-static approach, the resulting force on the panel is about 330.75 N. For a conservative check, the force is applied normal to the panel together with structural and panel weight. The load is transferred into the support through the actual panel connection points. Wind is of course time-varying in reality; here it is represented by a constant static force for a first strength and stiffness assessment rather than a gust or vibration analysis.

An automatic tetrahedral mesh is used with a global element size of about 5 mm. Local refinement is applied around the shaft holes, lower bracket connections, fillets and reinforced areas, where larger stress gradients are expected. Flat regions away from the connections can retain a coarser mesh to limit the total element count and solution time. The mesh is checked for severely distorted elements before solving. If the final combined load case produces a local peak stress, the mesh in that region should be refined further and the change in peak stress and deformation compared to confirm that the result is reasonably stable. Figure 3 shows the current finite-element mesh.

The static solution uses a single load step in which all loads act at the same equilibrium state. Structural weight is generated by gravity, while panel weight and wind are applied as equivalent external loads at the relevant connection regions. Before solving, the material, geometry and load units are checked carefully, particularly the conversion between Pa, MPa, N and mm. Welded or rigidly connected regions are treated as continuous, and the lower mounting surfaces are used as the restraint; bolt preload is not modelled separately. This level of simplification is suitable for an initial assessment of global strength and stiffness. A more detailed contact model can be introduced later if bolt-hole stress or interface slip becomes important. Table II summarizes the main settings for the static simulation.

DOI: 10.54254/2755-2721/2026.38120

Table 2. Main settings for the static simulation

Item	Simulation setting
Analysed component	Upper panel-support structure
Material	Q235 structural steel
Representative operating angle	30°
PV module weight	Approx. 294 N
Natural wind case	15 m/s, equivalent force approx. 330.75 N
Restraint	Fixed at lower mounting/connection surfaces
Mesh	Global size approx. 5 mm; local refinement at shaft holes and connections

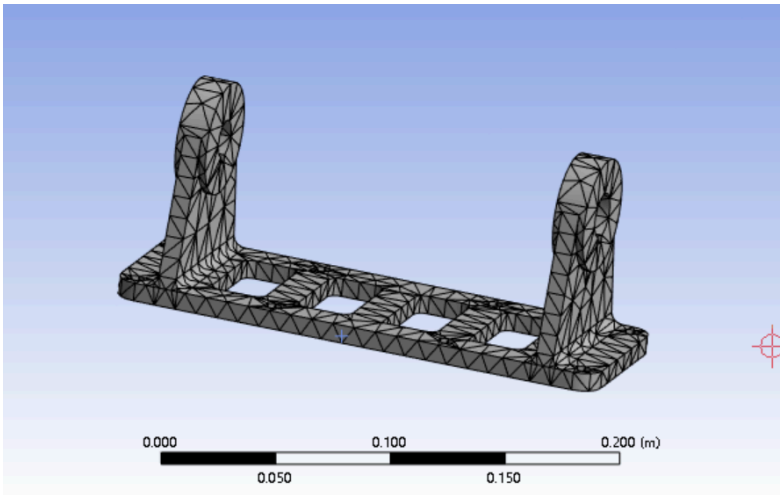


Figure 3. Finite-element mesh of the upper support structure

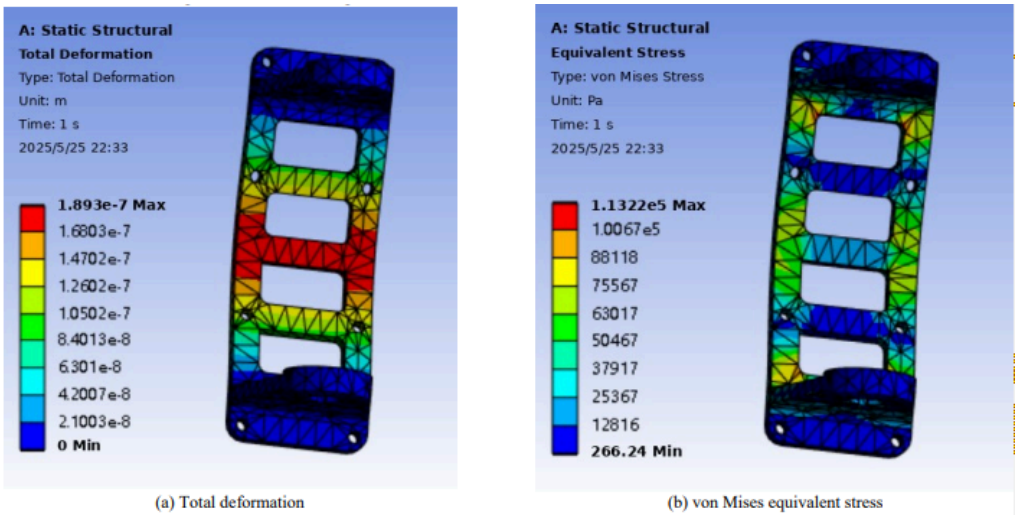
3.2. Stress and deformation analysis

After solving, the main outputs are von Mises equivalent stress and total deformation. The stress result is compared with the 235 MPa yield strength of Q235 steel, while total deformation is used as an indicator of structural stiffness. The location of the maximum deformation is as important as its magnitude because excessive displacement near the shaft can affect alignment, gear engagement or panel orientation. The contour plots are therefore examined around shaft-hole edges, plate corners, upright roots and fixed mounting regions rather than relying only on the single reported maximum. Very local peaks at sharp corners or idealised fixed boundaries are interpreted with care, as they may be numerical concentrations rather than representative structural stress.

The same units and comparable plotting ranges are used for each load case so that the colour scale does not become the basis for the safety judgement. For stress, the model-wide maximum is recorded first and then checked against its physical location. If the peak lies exactly at a fixed edge or sharp geometric corner, the surrounding element stresses are reviewed before treating it as a design value. For deformation, particular attention is given to the panel connection and elevation-shaft region because movement there is more likely to influence panel attitude and transmission

DOI: 10.54254/2755-2721/2026.38120

accuracy. The baseline and combined load cases are assessed in the same way so that the effect of wind can be compared directly. The available baseline stress and deformation contours are shown in Figure 4.



(a) Total deformation (b) von Mises equivalent stress

Figure 4. Static analysis results for the upper support structure

In the available baseline result, the maximum total deformation is approximately 1.89×10^{-7} m and the maximum von Mises stress is about 1.13×10^{5} Pa. Figure 4 shows that the larger responses occur mainly near connections and changes in geometry, while the rest of the support remains at a low stress and displacement level. Under this baseline load, the structure shows no meaningful deformation and the peak stress is far below the Q235 yield strength. The result also confirms that the geometry, constraints and mesh can be solved consistently and therefore provides a useful reference for the later combined case. Because the deformation is extremely small, the final analysis should still verify units, load transfer and restraint extent to rule out missing loads or excessive constraint.

Figure 4 comes from an existing baseline simulation file and does not contain a complete record of the 15 m/s wind acting together with panel self-weight. It should therefore not be treated as the final safety result for the wind-loaded case. The combined simulation should use the same material, mesh and restraints while adding wind to the existing gravity-related loads. This makes it possible to compare the change in peak stress, peak deformation and the locations of the most highly loaded regions. The design can only be judged against the intended operating condition once the combined case has been solved and the deformation at key connections remains compatible with normal bearing and gear operation.

After the combined case is solved, the factor of safety can be calculated from $n = \sigma_y/\sigma_{max}$, where $\sigma_y = 235$ MPa for Q235 steel and σ_{max} is the maximum von Mises stress under the combined load. A factor of safety above 1.5 is used here as a basic acceptance criterion together with the deformation result. This value indicates the remaining margin to yield, but it does not replace inspection of the stress location. High stress near shaft holes or bracket roots can be reduced by local thickening, larger fillets or reinforcing ribs. Excessive deformation along a long support segment can be addressed by increasing section depth or adding lateral bracing. If the lower connection carries a concentrated load, a larger connection plate or improved hole-to-edge spacing may be more effective.

DOI: 10.54254/2755-2721/2026.38120

The static study is therefore organised into two levels. The baseline case checks the model definition, material data, restraints and mesh and shows the basic response under self-weight. The combined case adds a 15 m/s natural wind to the same model to represent a more realistic outdoor condition. Both cases use the same output measures—maximum stress, maximum deformation and factor of safety—so the influence of wind can be compared directly. This structure also links the mechanical design clearly to the simulation evidence. Future work can extend the study to additional panel angles and higher wind speeds to examine how tracker posture affects the bracket response.

4. Conclusions

This study developed the mechanical structure of a dual-axis solar tracker and established a static-analysis framework for its main load-bearing support. The design uses separate azimuth and elevation motions. The upper assembly supports the PV module and controls panel tilt, while the lower azimuth stage provides horizontal rotation. Geared motors and spur gears transfer the drive torque. By defining the dimensions, materials and assembly relationships of the brackets, shafts, gears and base, a clear load path was established and the shaft holes, bracket connections and base mounting region were identified as key structural areas. The 3D model and component views also clarify how the two rotational stages work together.

The static analysis focuses on the upper panel-support structure, modelled in Q235 steel with restraints based on the actual mounting surfaces. The baseline case includes structural and panel self-weight, and the intended combined case adds a 15 m/s natural wind. In the available baseline simulation, the maximum total deformation is about 1.89×10^{-7} m and the maximum von Mises stress is about 1.13×10^{5} Pa, indicating very small structural response under the recorded load. Because the existing contour plots do not document the complete wind-loaded case, the final safety judgement still requires the same model to be solved with wind included and assessed using peak stress, deformation and factor of safety.

The gear-driven layout provides a clear relationship between motion and load transfer, and its main components can be produced using standard machining and off-the-shelf hardware. Once the combined wind case is completed, local high-stress regions can be refined through added thickness, larger fillets or reinforcement. Further simulations at different panel angles and wind speeds would show how operating posture changes the structural response. A physical prototype would provide an additional check of rotation, transmission stability and bracket deformation against the numerical results.

References

[1] Liu, B. M., Zhang, Q. H., & Zhao, Z. X. (2022). Design and implementation of a dual-axis sun-tracking photovoltaic system. *Application of Electronic Technique, 48*(4), 127–131. https://doi.org/10.16157/j.issn.0258-7998.211862. (in Chinese)

[2] Ren, J. W. (2022). Dual-axis coupled tracking photovoltaic power generation system based on IoT technology. *Automation & Instrumentation*(6), 40–46. https://doi.org/10.14016/j.cnki.1001-9227.2022.06.040. (in Chinese)

[3] Fang, L. R., Wang, L., Fan, L. J., Huang, Y. X., & Wei, N. (2024). Design of a dual-axis photovoltaic tracking system based on STM32. *Practical Electronics, 32*(6), 6–8. https://doi.org/10.3969/j.issn.1006-5059.2024.06.002. (in Chinese)

[4] Liu, X. Y., Zhu, J. R., Pan, Y., & Zhang, J. Y. (2024). Design of a photovoltaic tracking system based on Fourier fitting. *Southern Energy Construction, 11*(1), 54–63. https://doi.org/10.16516/j.ceec.2024.1.06. (in Chinese)

[5] Li, S. D., & Li, J. J. (2025). Design of a dual-axis photovoltaic tracking device based on an 8051 microcontroller. *Mechanical Research & Application, 38*(5), 79–81, 84. https://doi.org/10.16576/j.ISSN.1007-4414.2025.05.020. (in Chinese)

DOI: 10.54254/2755-2721/2026.38120

[6] Wu, C.-H., Wang, H.-C., & Chang, H.-Y. (2022). Dual-axis solar tracker with satellite compass and inclinometer for automatic positioning and tracking. *Energy for Sustainable Development, 66*, 308–318. https://doi.org/10.1016/j.esd.2021.12.013

[7] Mamodiya, U., & Tiwari, N. (2023). Dual-axis solar tracking system with different control strategies for improved energy efficiency. *Computers & Electrical Engineering, 111*, Art. no. 108920. https://doi.org/10.1016/j.compeleceng.2023.108920

[8] Pirayawaraporn, A., Sappaniran, S., Nooraksa, S., et al. (2023). Innovative sensorless dual-axis solar tracking system using particle filter. *Applied Energy, 338*, Art. no. 120946. https://doi.org/10.1016/j.apenergy.2023.120946

[9] Flores-Hernández, D. A., Islas-Estrada, L. R., & Palomino-Resendiz, S. I. (2024). A novel tracking strategy based on real-time monitoring to increase the lifetime of dual-axis solar tracking systems. *Applied Sciences, 14*(18), Art. no. 8281. https://doi.org/10.3390/app14188281

[10] Paliyal, P. S., Mondal, S., Layek, S., Kuchhal, P., & Pandey, J. K. (2024). Automatic solar tracking system: A review pertaining to advancements and challenges in the current scenario. *Clean Energy, 8*(6), 237–262. https://doi.org/10.1093/ce/zkae085

[11] Acosta-Banda, A., Aguilar-Esteva, V., Campos-Mercado, E., et al. (2025). Design, modeling, and experimental validation of a dual-axis solar tracking system with embedded control and monocular vision. *Energies, 18*(22), Art. no. 5951. https://doi.org/10.3390/en18225951

[12] Shang, H., & Shen, W. (2023). Design and implementation of a dual-axis solar tracking system. *Energies, 16*(17), Art. no. 6330. https://doi.org/10.3390/en16176330

[13] Alexandru, C. (2024). Simulation and optimization of a dual-axis solar tracking mechanism. *Mathematics, 12*(7), Art. no. 1034. https://doi.org/10.3390/math12071034

[14] Chen, H.-S., Lin, X.-Q., Hsu, C.-M., & Yang, C.-F. (2025). Fabrication of a dual-axis auto solar tracking system. *Sensors and Materials, 37*(6), 2421–2430. https://doi.org/10.18494/SAM5671

[15] Saber, A., Al Sharah, M., Al Tamimi, Y., Amine, S., & Hanna, E. G. (2025). Design, dynamic simulation, and prototyping of a dual-axis solar tracker using a slider-crank mechanism. *Engineering, Technology & Applied Science Research, 15*(5), 26224–26230. https://doi.org/10.48084/etasr.12414